Hot Corrosion Resistant Laser Coatings in Diesel Engine

J. Tuominen, M. Honkanen, M. Uusitalo, S. Ahmaniemi, P. Vuoristo, T. Mäntylä
Tampere University of Technology, Institute of Materials Science, Laser Application Laboratory, Tampere, Finland

Abstract

Hot corrosion tests have been conducted on Ni- and Cr-based laser coatings, a high-velocity oxy-fuel (HVOF) sprayed coating and various wrought alloys covered with a synthetic salt of Na_2SO_4-V_2O_5 and exposed at 650°C for 1000 h in air. Coating microstructures and reaction product layers were analyzed with scanning electron microscope (SEM) and energy dispersive spectrometer (EDS). The hot corrosion resistance of tested specimen was evaluated by measuring its mean thickness loss. Generally, wrought alloys, HVOF coating and Cr-based laser coatings suffered from selective corrosion beneath salt film, that is, distinct Cr-depleted layer was formed at alloy/salt interface. Cr-based laser coatings exhibited extended solid solubility and they transformed towards equilibrium condition. Cr-rich phases enriched further with Cr and they were prone to corrosion. Low diluted laser coatings and HVOF coating were more resistant to hot corrosion than commonly used industrial standard alloy, Nimonic 80A. Ni-based laser coating exhibited resistance equivalent to Cr-based coatings and superior to corresponding wrought alloy.

Introduction

Metals exposed to high temperatures (650 – 950 °C) suffer from hot corrosion at the presence of molten salt compounds, which destroys the protective oxide layer on metal surface. Deterioration usually proceeds rapidly and is unpredictable [1]. In big diesel engines (bore diameter normally ≥ 250 mm [2]) used in ships and stationary applications heavy fuels burnt in combustion chamber contain impurities of vanadium (V), sodium (Na) and sulphur (S). According to CIMAC (International Council on Combustion Engines) recommendations, fuel may contain V up to 600 mg/kg and S up to 45 g/kg as delivered [3]. Na introduced during the handling of fuel is usually at the level of 1 – 50 mg/kg [3, 4]. These elements are not fully carried away from the combustion chamber by exhaust gases but oxidize during

burning process (V_2O_5, Na_2O and SO_2/SO_3) in oxidizing environment and form salt compound deposits like Na_2SO_4 (sodium sulphate), V_2O_5 (vanadium pentoxide), $NaVO_3$ (sodium metavanadate) and other low melting point sodium vanadyl vanadates on the cooler walls of burning chamber by condensation from gas phase and by liquid droplet impact. Walls often exceed temperatures above which salt eutectics are molten. Uncontaminated sodium vanadyl vanadates are molten at the temperature of 535°C, however, according to [3, 5], metal oxides dissolved from the surfaces of corroding combustion chamber materials suppress the eutectic points even further down to 400 °C or well below. In addition to fuel-derived contaminants and reaction products like metal oxides (NiO, Fe_2O_3) and sulphates ($NiSO_4$, $FeSO_4$), such lubrication oil based compounds as calcium carbonate ($CaCO_3$) and calcium sulphate ($CaSO_4$) are often found in deposits on the basis of analyses taken from the several combustion chambers of commercially operated marine diesel engines [6-8]. Deposits, however, vary a lot according to the combustion conditions, temperature, pressure, fuel, location etc. [8].

Combustion chamber components, which are exposed to possible hot corrosion consists of piston crown, cylinder liner, cylinder head, exhaust and intake valves and fuel and water nozzles. Particularly vulnerable sites are those where long-term deposit formation can take place at high temperatures. These sites are flame faces of piston crown and exhaust valves. Since burning in combustion chamber is cyclic, temperatures on the walls of burning chamber vary as a function of time and location. During the period of combustion, the temperature of the piston crown has been reported to rise to the level of 330 - 400 °C [9, 10] and at the flame face of the valve up to 650 - 705 °C [11, 12]. Hot corrosion is also one contributory factor in cut/gap formation in seat areas of exhaust valves since temperatures are in the range of 360 – 575 °C [6-8, 12].

Hot corrosion resistance in molten salts including Na_2SO_4-V_2O_5 has been studied and reported for several commercial

metal alloys and coatings prepared by conventional methods like flame, arc, plasma and HVOF spraying and arc welding [7, 13, 14]. Common to the results is that the most significant alloying element to combat hot corrosion is Cr. Moreover, laser remelting has improved the hot corrosion resistance of sprayed metallic coatings substantially. In addition to metallic coatings, ceramic coatings are potential combustion chamber materials due to their superior hot corrosion and erosion resistance and potential to enhance efficiency of the engine by lowering the heat losses [12]. Hot corrosion of thermal barrier coatings (TBCs) have been studied and tested in diesel engines for instance in [15, 16]. Spallation of the coatings and reactivity of yttria, magnesia and calcia with sulphur, sodium and vanadium contaminants have been encountered.

The current trend in marine diesel engine manufacturing is towards higher efficiency and lower emissions. Due to future exhaust emission restrictions, the use of low-sulphur fuel will increase and hence corrosion problems are expected to decrease. On the other hand, in order to increase the engine power per cylinder, operating temperatures and pressures in combustion chambers are set higher. This places higher demands not only on lubrication but also on combustion chamber materials in corrosion point of view. Laser cladded metallic coatings are potential candidates to combat hot corrosion problems in combustion chamber environments, increase the time between overhauls and even replace the use of expensive Nimonic alloys, as laser cladding and coatings have some prime advantages like metallurgical bond, low dilution, low heat input and high integrity compared to conventional coatings. Schlager et al. [17] already applied several Ni-based laser coatings on the flame faces of marine diesel engine exhaust valves made of Nimonic 80A and tested them in real service conditions. They stated that laser coatings showed better hot corrosion resistance than Nimonic 80A, but coatings, 1 – 2 mm in thickness, corroded away before overhaul.

In this study, two Cr-based alloys (Fukuda SX-707, SX-717) and a Ni-based superalloy (Inconel 625) were deposited onto 42CrMo4 QT steel by HPDL cladding process. Hot corrosion properties of laser coatings, HVOF sprayed coating (SX-707) and four Ni- and Fe-based alloys namely superalloys Nimonic 80A, Inconel 625, Inconel 718 and 42CrMo4 QT steel were tested in $Na_2SO_4–V_2O_5$ at 650°C for 1000 h in air environment. The aim of this simple laboratory test was to select potential coating material and method for marine diesel engine tests. They could be applied primarily on top of piston crown made of QT steel and secondarily onto Fe-based water injection nozzle and flame face of Fe-based exhaust valve.

Experimental

Three commercial Ni- and Cr-based alloy powders were deposited onto grit-blasted 42CrMo4 QT steel (AISI4142) substrates (thickness 20 mm, 250 $HV_{1.0}$) by using one-step

Table 1: HPDL cladding parameters for Inconel 625, SX-707 and SX-717.

Power	4.8 kW
Traverse speed	300-350 mm/min
Powder feed rate	68-100 g/min
Shielding gas (Ar)	50 l/min
Track width	20 mm

Table 2: HVOF spraying parameters for SX-707.

Oxygen	240 l/min
Propane	70 l/min
Air	375 l/min
Powder feed rate	60 g/min

laser cladding method. Rofin-Sinar (Rofin-Sinar Laser GmbH, Hamburg, Germany) DL060H2 6 kW direct high power diode laser (HPDL) mounted to KUKA (KUKA Roboter GmbH, Augsburg, Germany) KR125 robot system was used as a power source. Laser beam exhibited homogenous energy density distribution in direction perpendicular to cladding direction and Gaussian distribution in cladding direction. Laser was equipped with off-axis nozzle configuration. Laser cladding parameters used for different powders are shown in Table 1.

SX-707 coating was sprayed with Diamond Jet Hybrid 2700 HVOF spray gun onto alumina (grit 32) grit-blasted 42CrMo4 QT steel (AISI4142) substrate (thickness 10 mm). The spraying parameters used are shown in Table 2.

Test specimens to hot corrosion tests were prepared by cutting to the size of 10 x 15 x 10 mm^3. Laser coatings were ground with grinding machine. HVOF sprayed coating and wrought samples were ground manually with SiC paper grit 600. In order to prevent the material loss from the backside of the samples and make it easier to measure the thickness losses after the test, the backsides of each test specimen were HVOF sprayed with the layer of SX-707 of 0.4 mm in thickness. Before and after the test, the sample thickness was measured from the interface of backside coating to the free surface of the grounded/corroded test coating. Thickness measurements, average of 12 measurements, were performed with optical microscope equipped with a measuring table.

The specimens prepared to hot corrosion tests were covered with a controlled amount of $Na_2SO_4–V_2O_5$ synthetic salt and placed on alumina crucibles in Lindberg/Blue M vertical tube furnace. Two specimens of each material were exposed to 650 °C for 1000 hours. After every 100 hours the mixture of $Na_2SO_4–V_2O_5$ in powder form and liquid ethanol (C_2H_5OH) were added on top of specimens, approximately 100 mg at a time. Furnace was always cooled down before the salt was added. Air was blown to the furnace at a rate of 1 l/min during the test.
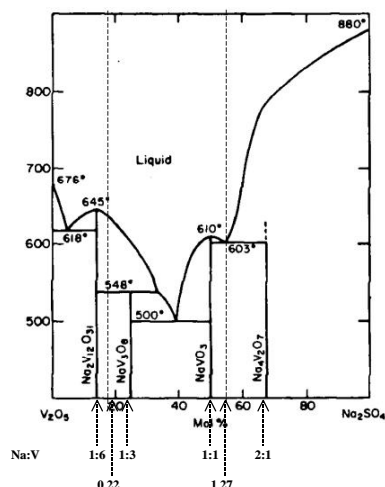
Figure 1: Phase equilibrium for Na_2SO_4-V_2O_5 [18].

The salt consisted of $50Na_2SO_4$-$50V_2O_5$ (wt.%), which was $56Na_2SO_4$-$44V_2O_5$ (mol.%, Na:V; 1.27). According to equilibrium phase diagram shown in Fig. 1, the compound was in molten state during the test [18]. In order to identify the forming sodium vanadyl vanadates, the salt mixture was exposed at 650 °C for 5 hours in stagnant air after which it was cooled down slowly in furnace. The compounds formed were determined by XRD. It revealed the presence of NaV_6O_{15} (Na:V; 1:6, T_m = 625°C) and Na_2SO_4. As a reference, formed compounds of $18Na_2SO_4$-$82V_2O_5$ (mol.%, Na:V; 0.22) salt consisted of NaV_6O_{15}. $NaV_6O_{15} = Na_2O \cdot V_2O_4 \cdot 5V_2O_5$ sodium vanadyl vanadate, commonly known as 1.1.5 NaVV, is one of the most frequently found composition deposited on an exhaust valve [6]. As Bryers explained sodium vanadyl vanadates could be formed between Na_2SO_4 and V_2O_5 by reaction as follows [19]:

$$xNa_2SO_4 + yV_2O_5 = (Na_2O)_x \cdot yV_2O_5 + xSO_3$$

Reaction was apparently not finished after 5 hours at 650 °C, as Na_2SO_4 was still present in Na:V; 1.27 salt. EDS analysis taken from the Na:V; 0.22 salt confirmed that sulphur reacted fully into SO_3.

After the hot corrosion tests, the specimens were mould into cold-setting resin. Resin buttons were then cut in half to reveal the cross sections. Next, the specimens were ground and polished in dry condition during the metallographic preparation in order to prevent the dissolution of possible water-soluble reaction products like sulphates of Na and Ni. Prepared cross-sections were then carburized and examined by SEM and EDS.

Results and Discussion

Coatings

Inconel 625 laser (63Ni-22Cr-9Mo-4Nb-1Fe-0.5Mn-0.5Si): Laser coating exhibited very dense and crack-free columnar
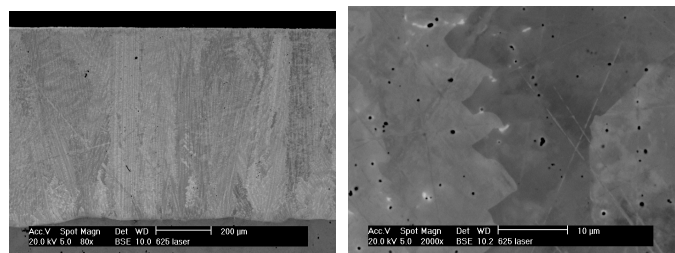

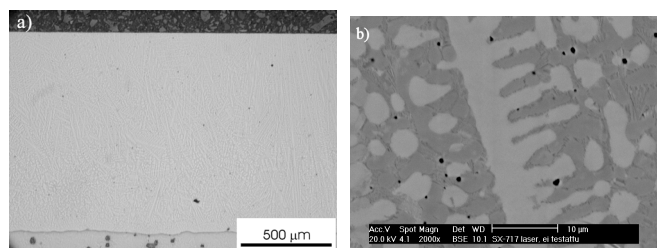Figure 2: BSE images of Inconel 625 coating.

Figure 3: SX-717 laser coating; a) optical micrograph and b) BSE image. Light areas are rich in Cr and Mo compared to composition of initial powder.

and dendritic (very short secondary arms) microstructure strongly welded to the substrate. Mo- and Nb-rich precipitates were detected abundantly. Some small black dots irregular in shape were also detected in BSE image. EDS point and line scan analyses revealed that they were rich in Ti. Smaller spherical black dots were probably micropores. Compositional difference between light and dark phases was not detected (Fig. 2). Compositional dilution was only 2 %. It was calculated according to [20]. Heavily and increasingly diluted zone in the coating next to interface was neglected. Width of this zone at the centre of track was 160 μm according to line scan analysis. Microhardness of the coating was at the level of 250 $HV_{0.3}$. The HAZ of the substrate hardened to 630 $HV_{1.0}$.

SX-717 laser (42.5Ni-53.5Cr-2.5Mo-1Si-0.5B): Laser coating exhibited very dense and crack-free dendritic (more obvious than in Inconel 625) microstructure strongly bonded to the substrate. Segregation of phases took place as is shown in Fig. 3. The average composition (wt.%) of Cr-rich dendritic phases was 35Ni-59Cr-3Mo-1Si-2Fe and interdendritic Ni-rich phases 47Ni-48Cr-2Mo-1Si-2Fe. Alloy exhibited extended solid solubility, since Ni-phase dissolved more Cr and Cr-phase more Ni than expected according to binary Ni-Cr equilibrium phase diagram. Compositional dilution was only 2 %. Microhardness of the coating was at the level of 575 – 590 $HV_{0.3}$.

SX-707 laser (45Ni-51Cr-3Mo-1Si): Laser coating exhibited identical microstructure to SX-717 laser coating except for compositional dilution, which was 6 %. Microhardness was at the level of 460 – 470 $HV_{0.3}$.
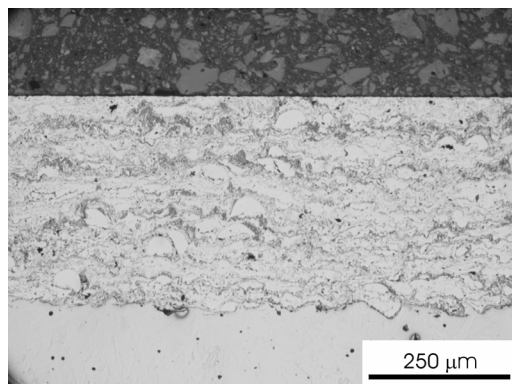
Figure 4: Optical micrograph of SX-707 HVOF coating.

SX-707 HVOF (45Ni-51Cr-3Mo-1Si): HVOF spraying method produced layered coating microstructure typical for sprayed metallic coatings (Fig. 4). Inter-splat boundaries can be clearly distinguished due to oxide layers at splat boundaries. Most of the splats are wide and relatively flat, however surprisingly high amount of round not fully melted splats were detected. General impression is that the coating was not very dense. Microhardness of the coating was at the level of 490 – 510 $HV_{0.3}$.

Hot Corrosion Tests at 650°C for 1000 Hours
According to thickness loss measurements shown in Fig. 5, all the tested laser coatings and HVOF coating exhibited good resistance to hot corrosion. The coatings resistance appeared to be even slightly better than Nimonic 80A and much better than other wrought reference alloys. Hot corrosion morphology of tested specimens was generally characterized by thick, porous layers of oxides with the underlying alloy depleted in Cr. Microstructures and reaction product layers of coatings and wrought alloys are shown and discussed in details as follows.

SX-707 HVOF (45Ni-51Cr-3Mo-1Si): Deterioration of HVOF coating was not uniform. Some wide and shallow pits were clearly detected on the coating surface beneath the reaction product layers. However, most importantly, elements of salt did not penetrate through the splat boundaries into the coating and substrate indicating that coating was dense enough to keep it intact for this particular test environment. Cr-depleted zone in coating was formed near the top surface. Sulfur was absent in the reaction product layer. Internal sulfidation, however, frequently takes place in materials, which suffer from hot corrosion. L_a-lines of Mo overlap the K_a-lines for S, which made it difficult to be conclusive was there any S in the coating.

SX-717 laser (42.5Ni-53.5Cr-2.5Mo-1Si-0.5B): The coating exhibiting the best hot corrosion resistance deteriorated uniformly. Reaction product layers were similar to those in SX-707 produced with HVOF. BSE image revealed that areas rich in Cr and Mo were more heavily deteriorated than Ni-rich
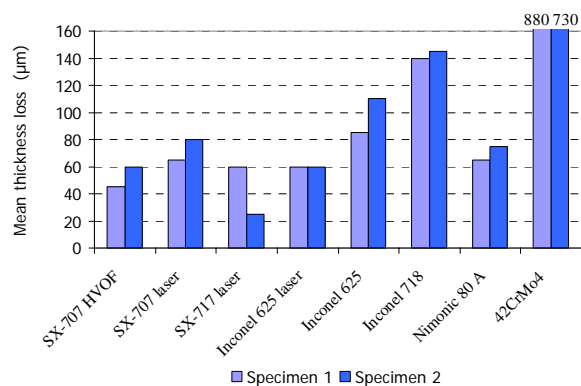

Figure 5: Thickness loss measurement results of specimens exposed to Na_2SO_4-V_2O_5 (50/50 wt.%) (Na:V=1.27) in air at 650°C for 1000 h.

areas. These areas appear dark in Figs. 6 and 7. It was also observed that Cr-rich phases enriched further with Cr. The average compositions (wt.%) of Cr- and Ni-rich phases were 32Ni-63Cr-3Mo-1Si-1Fe and 48Ni-47Cr-2Mo-1Si-2Fe, respectively. Uusitalo noticed earlier that Cr-rich phases in high-Cr NiCr laser coatings were prone to chlorine attack [21].

SX-707 laser (45Ni-51Cr-3Mo-1Si): Degradation of the coating was similar to SX-717 laser coating. Thickness loss was notably higher than in HVOF coating apparently due to higher iron content as a result of dilution.

Inconel 625 laser (63Ni-22Cr-9Mo-4Nb-1Fe-0.5Mn-0.5Si): Inconel 625 laser coating deteriorated uniformly as illustrated in Fig. 8. Reaction product layer was stratified to several thin layers unlike that in Cr-based coatings. In general, it was more homogenous than in Cr-based coatings. Despite Cr-rich reaction product next to the coating, no distinct Cr-depleted zone was detected in the coating (Fig. 9).

Inconel 625 wrought (63Ni-22Cr-9Mo-4Nb-1Fe-0.5Mn-0.5Si): Deterioration of the surface was uniform, that is, no preferential grain boundary attack was detected, as shown in Fig. 10. Distinct and uniform Cr-depleted layer of approximately 3 μm thick was now formed in alloy just beneath the reaction product layer (Fig. 11), which was similar to that in the corresponding laser coating except for some Mo- and Nb-rich areas detected.

Nimonic 80A wrought (Ni-20Cr-3Fe-2Co-2Ti-1Al): Deterioration of Nimonic 80A was uniform across the specimen surface. The reaction product layer was clearly divided into rather dense Cr-rich layer near the salt/alloy interface and porous upper layer, which was rich in Ni. Layer next to salt/alloy interface was strongly stratified as shown in Figs. 12 and 13. Cr-depleted layer, approximately 7-13 μm in thickness, was formed in the alloy next to reaction product interface. Grain boundaries, which are clearly seen in Fig. 12, did not contain any corrosive species. Instead, sulphur was
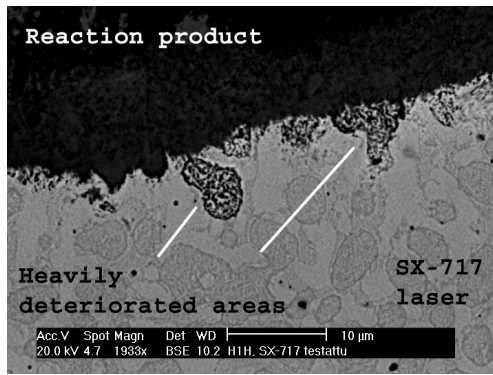
Figure 6: Cross-section of SX-717 laser coating reacted at 650°C in air with $Na_2SO_4 - V_2O_5$ (50/50 wt.%) (Na:V = 1.27) on the surface.

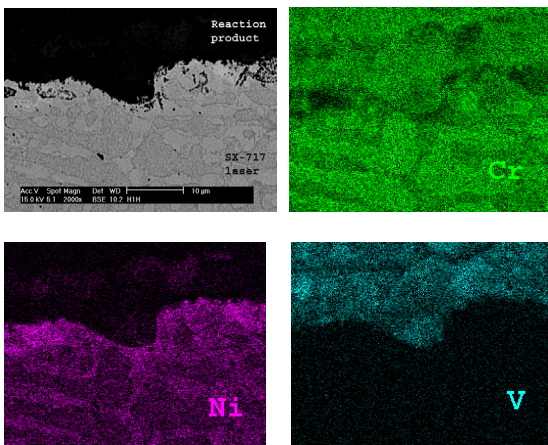*Figure 7. Elemental maps of SX-717 laser coating.*

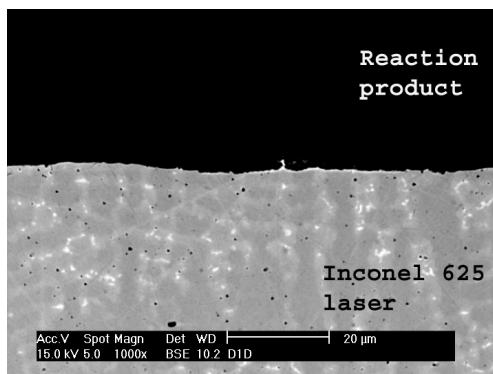*Figure 8: Cross-section of Inconel 625 laser coating reacted at 650°C in air with $Na_2SO_4 - V_2O_5$ (50/50 wt.%) (Na:V = 1.27) on the surface.*

detected on the bottom of Cr-depleted layer indicating that internal sulfidation caused by Na_2SO_4 has taken place. In this case, S cannot be mixed with Mo since Nimonic 80A does not contain Mo.

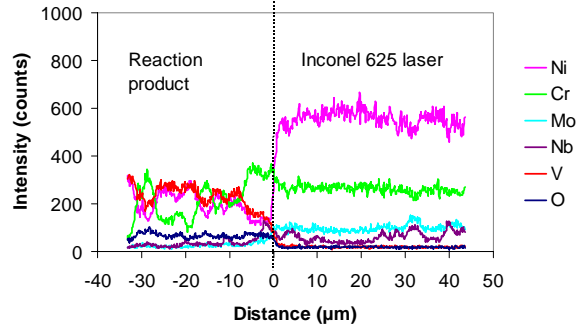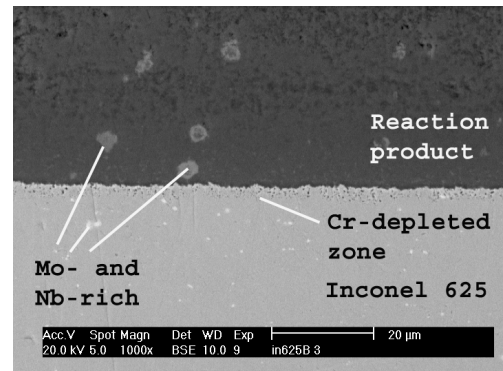*Figure 9: Line scan of Inconel 625 laser coating.*

Figure 10: Cross-section of wrought Inconel 625 reacted at 650°C in air with $Na_2SO_4 - V_2O_5$ (50/50 wt.%) (Na:V = 1.27) on the surface.
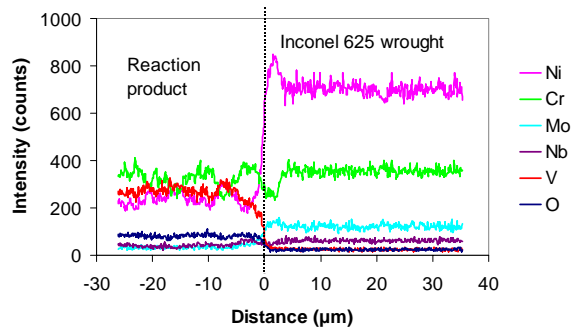

Figure 11: Line scan of wrought Inconel 625.

Conclusions

Vanadic hot corrosion tests have been conducted on Ni- and Cr-based laser coatings, HVOF sprayed coating and various wrought alloys. Low diluted laser coatings and HVOF coating were more resistant than Nimonic 80A. Inconel 625 laser coating exhibited resistance equivalent to Cr-based coatings and superior to corresponding wrought alloy. Metastable Cr- and Ni-rich phases segregated in Cr-based laser coatings. Cr-rich phases enriched further with Cr during the test and they were prone to hot corrosion.
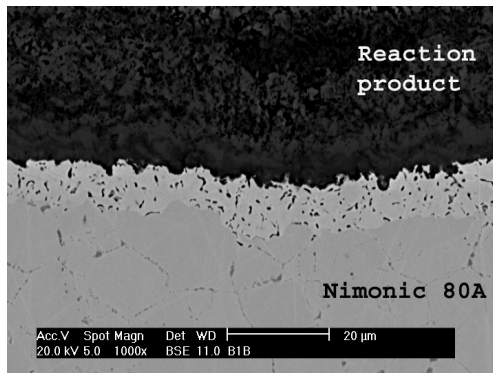
Figure 12: Cross-section of wrought Nimonic 80A reacted at 650°C in air with $Na_2SO_4 – V_2O_5$ (50/50 wt.%) (Na:V = 1.27) on the surface.
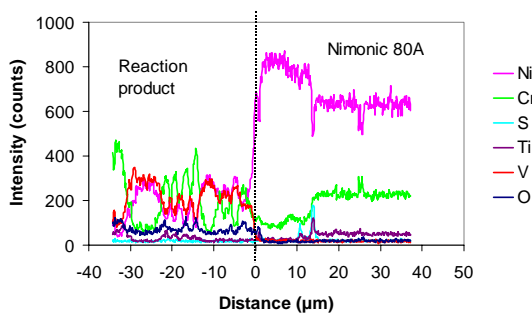

Figure 13: Line scan of wrought Nimonic 80A..

References

1. N. Eliaz, G. Shemesh and R. M. Latanision, Hot corrosion in gas turbine components, *Engineering Failure Analysis,* Vol 9, 2002, p. 31-43

2. B. Challen and R. Baranescu, *Diesel Engine Reference Book,* 2nd ed., Butterworth-Heinemann, Oxford, UK, 1999, p. 120

3. "CIMAC: Recommendations regarding Fuel Quality for Diesel Engines", (No. 21), CIMAC, Frankfurt, Germany, 2003, Revised 2004-04-05

4. K. Aabo, CIMAC Heavy Fuel Oil Working Group, and Experience from Operation on Today's Fuels and Low-sulphur Fuels, *24th International Bunker Conference*, Hilton Hotel in Rotterdam, Netherlands, 7-9 May 2003

5. P. Kofstad, *High Temperature Corrosion*, Elsevier Applied Science Publishers Ltd, Essex, UK, 1988, p. 495

6. S. K. Nanda and A. P. Roskilly, Exhaust valve failure under residual fuel operation, *Journal of Marine Design and Operations*, (No. B2), 2003, p. 23-28

7. J. R. Nicholls, Coatings and hardfacing alloys for corrosion and wear resistance in diesel engines, *Materials Science and Technology*, Vol 10, 1994, p. 1002 – 1012

8. T. Takase, M. Yamawaki, M. Takahashi, T. Inoue, K. Shinbori, Y. Kon and H. Oida, Investigation Results for Combustion Residue of Marine Diesel Engines, *Bulletin of the M.E.S.J.*, Vol 27 (No. 1), 1999, p. 29-38

9. S. Mizuhara, M. Kunimitsu, O. Beppu, M. Takahashi, A. Sakane and M. Tanaka, High-Powered ADD3OV Medium Speed Diesel Engine, *Bulletin of the M.E.S.J.*, Vol 27 (No. 2), 1999, p. 65-73

10. K. Aeberli, Experience with Sulzer Common-Rail Engines, *25th Motorship Marine Propulsion Conference*, Hamburg, Germany, 7 – 8 May 2003

11. H. Fellmann, T. Gross and T. Ludwig, Typical wear mechanism of 2-stroke exhaust valves, *Proceedings of the Marine Propulsion Conference*, Amsterdam, Netherlands, April 28-29, 2004

12. J. W. Fairbanks, E. Demarey and I. Kvernes, Insulative, wear and corrosion resistant coatings for diesel and gas turbine engines, *Surface Engineering: Surface Modification of Materials*, Kossowsky, R., Singhal, S. C., Les Arcs, France, 3–15 July, 1983, 1984 p. 524-545

13. Y. Longa and M. Takemoto, Laser Processing of High-Chromium Nickel-Chromium Coatings Deposited by Various Thermal Spraying Methods, *Corrosion,* Vol 50 (No. 11), 1994, p. 827-837

14. H. S. Sidhu, B. S. Sidhu and S. Prakash, Hot Corrosion Behaviour of HVOF Sprayed Coatings on ASTM SA 213-T11 Steel, *Building on 100 Years of Success*, B. R. Marple, M. M. Hyland, Y. C. Lau, R. S. Lima, J. Voyer, Eds., May 15-18, 2006, (Seattle, Washington, USA), ASM International, Materials Park, OH, USA, 2006

15. I. Kvernes, O. Norholm and J. Svartdal, *Ceramic coatings' influences on medium speed diesel engine performance and reliability*, Diesel Engine Combustion Chamber Materials for Heavy Fuel Operation, DTI/Industry Valve Project 1990, the Institute of Marine Engineers, London, UK, 1990, p. 99-104

16. S. Ahmaniemi, J. Tuominen, P. Vuoristo and T. Mäntylä, Sealing Procedures for Thick Thermal Barrier Coatings, *Journal of Thermal Spray Technology*, Vol 11 (No. 3), 2002, p. 320-332

17. D. Schlager, C. Theiler and H. Kohn, Protection against high temperature corrosion with laser welded claddings – Applied and tested on exhaust valve discs of large diesel engines burning heavy fuel oil, *Materials and Corrosion* 53, 2002, p. 103-110

18. R. S. Roth, T. Negas and L. P. Cook, *Phase Diagrams for Ceramists*, Vol. IV, Fig. 5127, The American Ceramic Society, Columbus, OH, USA, 1981, p. 89

19. R. W. Bryers, Fireside slagging, fouling, and high-temperature corrosion of heat-transfer surface due to impurities in steam-raising fuels, *Prog. Energy Combust. Sci.,* Vol 22, 1996, p. 29-120

20. E. Toyserkani, A. Khajepour and S. Corbin, *Laser cladding*, CRC Press LCC, 2005, Boca Raton, NC, USA, p. 32

21. M. Uusitalo, "High temperature corrosion and erosion-corrosion of coatings in chlorine-containing environments", Doctoral Thesis, Tampere University of Technology, 2003, p. 45